ANALYSIS, INTERPRETATION, AND MODELING OF MARS DAYGLOW SPECTRA. D. L. Huestis[1], T. G Slanger[2], B. D. Sharpee[2], P. C Cosby[2], and J. L. Fox[3], [1]SRI International, Menlo Park, CA 94025, david.huestis@sri.com, [2]SRI International, Menlo Park, CA 94025, [3]Wright State University, Dayton OH, 45435.

Introduction: The Mariner 6 and 7 (1969), Mariner 9 (1971), and Viking 1 and 2 (1975) missions provided the first quantitative details about the structure and energetics of the Mars atmosphere [1-8]. These limited data sets supplied the observational foundation for the current semiempirical reference atmospheric models [2, 10-13]. Not until more than 20 years later did new generations of landers and orbiters begin to revisit the planet [14-24].

The Mariner spacecraft had UV spectrometers that recorded limb scans of the Mars dayglow spectrum, shown in Figure 1, versus tangent ray height. The primary objective of the work reported here is comparative analysis, interpretation, and modeling of the altitude profiles of the Mars dayglow as recorded during the Mariner and Mars Express (MEX) Missions.

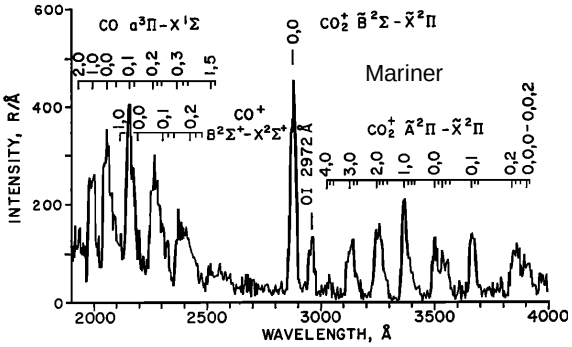

Figure 1: The Mars dayglow spectrum as recorded by Mariner 6 and 7 flyby missions [1]. The Mariner 9 [4,5] and the MEX SPICAM [22] spectra are similar in overlapping wavelength regions.

Altitude profile of the Mars atmosphere: Before attempting to interpret and model the altitude profiles of the dayglow emissions, we first need to examine what we know from direct observations about the mass density and composition of the ambient Mars atmosphere.

Mazarico et al. [18] gave a good discussion of the heritage of current Mars atmosphere "reference" models [2, 10-13]. They point out that the Mars exospheric temperature is only weakly constrained by direct observations. A second important issue is that the observed mass density profiles versus altitude show abrupt jumps in mass density over a few kilometers of altitude change. These mass density excursions are reflected in the retrieved temperature profiles and are often rationalized as being due to waves or tides [25-28]. A third issue is that the numerical process of extracting the pressure and temperature profiles amplifies the statistical fluctuations and measurement errors in the recorded mass profiles [9].

In the present case we are less interested in temperature, pressure, waves, tides, and the details versus ground location and season. Limb observations of airglow and UV occultation represent integral averages over ground location and altitude. What we really want is a simple working model of the composition of the ambient atmosphere, with only a few adjustable parameters, and smoothed altitude resolution, to help us identify the precursors of the airglow emissions. Such simple quasi-static models [29] have been useful for semiquantitative studies of the Earth's atmosphere.

Our reanalysis began with log-linear fits to published tabulated and graphical data. The preliminary results are summarized in Table 1.

Table 1: Mars atmosphere mass density scale heights.

Mission	Altitudes (km)	H (km)	Ref's
Viking 1	140–190	10–11	[6], [7]
Viking 2	140–174	8	[6], [7]
MGS	110–140	7.1	[14]
Mars Odyssey	103–160	6.4 & 8.8	[17]
Spirit	100	7.1	[24]
MEX	100–120	6.5	[23]
MEX	100–130	7.1	[21]
MEX	50–100	7.8	[21]

A more robust approach is illustrated by following simplified analysis of the Spirit lander data. As noted by Withers and Smith [24], the temperature profile derived from the Spirit accelerometer data shows much less violent jumps and oscillations than those from the other four landers, suggesting that it might be adequately represented by a convenient functional form. We began with the simplest choice of a constant temperature lapse rate, $T(z) = T_0 - L_0 z$, for which the hydrostatic equilibrium differential equation is solvable analytically.

This constant-lapse approach was used to fit the Spirit accelerometer data from 0 to 90 km, with T_0 = 228 K and L_0 = 0.96 K/km. The residuals are shown as the right-hand curve in Figure 2. Note that removal of the baseline altitude trend shows that even noisy data have something to offer. Note also the abruptness of the mass density excursions in the Pathfinder data at 65 and 85 km. Something really interesting is happen-

ing at altitudes between 85 and 110 km, and has been for more than 30 years.

Better fits to the descent data could have been obtained by using a more complicated functional forms for the assumed temperature profiles, such as piecewise linear representations of T(z) or 1/T(z), and Pade-approximates (ratios of polynomials).

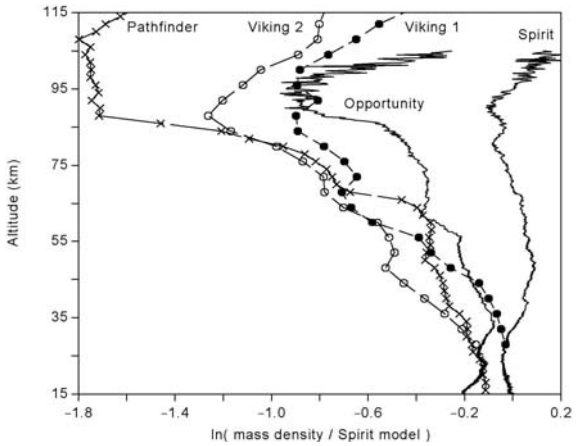

Figure 2: Analysis of mass density altitude profiles as recorded by mass spectrometry and accelerometry by five Mars landers: *Viking 1*, filled circles and dashed lines [6,7]; *Viking 2*, open circles and dashed lines [6,7]; *Pathfinder*, × symbols and long dashed lines [16]; *Opportunity* and *Spirit*, solid lines [24]. Each lander data set has been normalized to a reference altitude profile called the "Spirit Model" (see the text). The *Viking 1* data have not yet been shifted downward by 1.3 to 2.4 km, as was recommended by Withers et al. [8].

Subtracting Dust-Scattered Sunlight: Figure 3 illustrates that at wavelengths longer than 250 nm solar radiation features increasingly contaminate the dayglow spectrum as the tangent ray height is reduced below 130 km. Stellar occultation measurements have shown that there is haze opacity up to 100 km [30]. Depending on the details of the baffling of the spectrometer inlet, the recorded spectrum may include sunlight scattered by dust or clouds at much lower altitudes. The problem is especially severe at Venus, where clouds that were nominally around 60 km altitude interfere with low-wavelength dayglow observations until the tangent ray heights were above 150 km [31]. Figure 3 illustrates that there is valuable information about CO_2^+(B-X) doublet at 289.0 nm and the O(^{1}S-^{3}P) atomic line at 297.2 nm if we can subtract the solar contribution. To do so we made a model of the solar spectrum in this region and subtracted its contribution to the dayglow spectrum, allowing us to track the 289.0 and 297.2 nm emissions down to below 80 km. These lower altitude data will be included in our discussion of dayglow altitude profiles below.

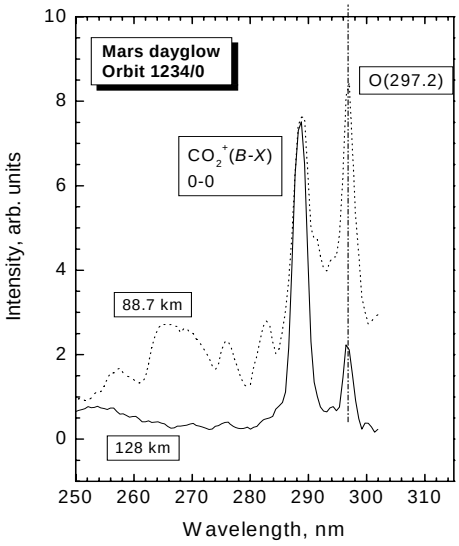

Figure 3: SPICAM spectra of Mars dayglow at low altitude and long wavelength. Features from the solar spectrum become more evident at lower altitudes, but the CO_2^+ doublet and the O(^{1}S) line are still discernible.

Dayglow Altitude Dependence: Figure 4 illustrates graphically the altitude dependence of the prominent Mars dayglow emissions. The open square symbols represent the data from the Mariner 6 and 7 missions [1,2], while the open diamond symbols represent the Cameron Band emissions recorded by the Mariner 9 mission [3-5]. The filled symbols come from MEX SPICAM observations, with the Cameron Band data coming from co-added MEX SPICAM data from Leblanc et al. [22] ("star" symbols in Figures 7a and 7b therein), and the other two emissions from SRI re-analysis of low-altitude MEX SPICAM data to remove scattered sunlight [32], as described above.

The three straight lines represent linear least squares fits, each assuming constant mass scale heights. The logarithmic intensity scales for the various data sets were individually shifted slightly to minimize the overall $\chi^{(2)}$. The observed emission intensities were each clearly exponential over relatively large ranges of altitude, which motivates consideration of what can be inferred from the fitted exponential scale heights, H.

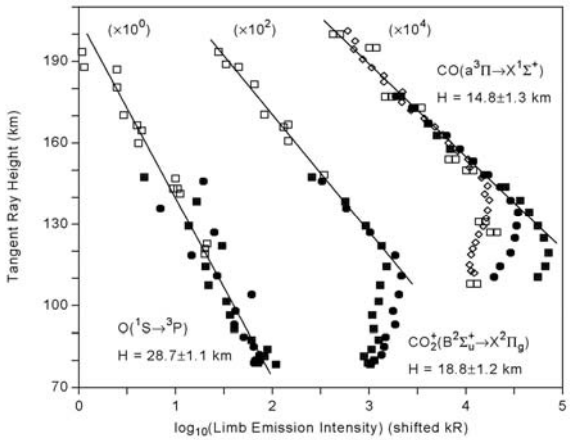

Figure 4: Altitude profiles of dayglow emissions on Mars. Open symbols from Mariner 6, 7, and 9 observations. Filled symbols from MEX SPICAM observations.

Mechanistic Implications: The Mariner dayglow observations motivated numerous modeling studies and laboratory experiments that contribute to quantitative understanding of one of the possible underlying collisional and photochemical production mechanisms (which we do not have space to review in detail here). The most obvious source reaction is photodissociation of ambient CO_2, which is known in the laboratory to produce all four dayglow emitting states:

$$h\nu + CO_2 \rightarrow O(^1S), CO(a^3\Pi), CO_2^+(A^2\Pi_u \,\&\, B^2\Sigma_u^+)$$

If this simplest of models were sufficient, then the high altitude dayglow emissions would all share the same scale height, which would be that of CO_2. Comparison of the scale heights within Figure 4 and with those in Table 1, shows that the dayglow scale heights are definitely not the same as each other (Figure 4), and that all three are significantly larger than that of CO_2 (see Table 1).

Additional source reactions were suggested in the original Mariner 6 and 7 publication [1]: e + CO_2, e/hν + CO, and e/hν + CO_2^+. These source reactions were supplemented by others in the first comprehensive model of the Mars dayglow, published by Fox and Dalgarno in 1979 [33], using the best laboratory data then available. The resulting modeled high-altitude scale heights for the key source reactions are indicated in columns 1 and 2 of Table 2.

Table 2: Comparison of scale heights (in km) for modeled excited state production reactions (columns 1 and 2, from the work of Fox and Dalgarno, FD79, [33]), and observed scale heights of the observed dayglow emissions (columns 3-5, from Figure 4 above).

Reaction	H[FD79]	H[O(^{1}S)]	H[CO_2^+(B)]	H[CO(a)]
hν + O	28	29		
e + O	17-26	29		
hν + CO_2^+	19		19	
e/hν + CO	14			15
e + O_2^+	13	29		
e + CO_2^+	11	29		15
e/hν + CO_2	10	29	19	15

In Table 2 the scale heights for the dayglow emissions (columns 3-5) are written in the rows for their possible source reactions. Thus O(^{1}S) could be produced by one or more of six possible source reactions (note that e/hν + X counts as 2 reactions). Correspondingly, $CO_2^+(B^2\Sigma_u^+)$ could be produced in three reactions and CO($a^3\Pi$) in five. Comparison of columns 3-5 with column 2 in Table 2 suggests that for all three dayglow emissions there is a single dominant precursor species at high altitude: O(^{3}P) for O(^{1}S), $CO_2^+(X^2\Pi_g)$ for $CO_2^+(B^2\Sigma_u^+)$, and CO($X^1\Sigma^+$) for CO($a^3\Pi$); in each case the corresponding ground state species.

Current models [34,35] follow approaches similar to those used by Fox and Dalgarno [33]. Many excitation processes are included, some with weakly constrained parameters. The resulting dayglow altitude profiles respresent a superposition of the altitude dependences of the source reactions. None of these models does an adequate job of describing the observational data summarized in Figure 4 and Table 2. For example, the modeled altitude dependence of O(^{1}S) emission [Ref 33, Figures 12 and 13] is quite different from what has been observed by the Mariner and MEX missions. The model profile is double peaked (at about 90 and 130 km) and has a high-altitude scale height of about 11.5 km. In contrast, the observational data, shown in Figure 4 above, show no evidence of a peak, and has a scale height of about 28.7 km. The more complicated *Trans-Mars* model described in the preprint by Simon et al. [34] appears to plausibly represent the altitude dependence of the CO(a-X) and the CO_2^+(B-X) emissions from about 115 to 160, but the linear range is too short to extract reliable scale heights from the rather noisy data. In contrast, the Monte Carlo model of Shematovich et al. [35] does a plausible job of calculating the altitudes of the peak CO(a-X) and CO_2^+(B-X) emissions, but is very poor on calculat-

ing the scale heights in the exponential-decrease regions.

Summary and Conclusions: After simultaneous analysis of dayglow data from the Mars Express SPICAM instrument and much older data from the Mariner 6, 7, and 9 missions, the altitude profiles for the $O(^1S\text{-}^3P)$, $CO(a^3\Pi\text{-}X^1\Sigma^+)$, and $CO_2^+(B^2\Sigma_u^+ \rightarrow X^2\Pi_g)$ dayglow emissions are now much better defined and provide more demanding challenges to models of the Mars atmosphere from 80 to 200 km.

It is now time to reexamine assumptions made in construction of previous and current models and the reliability of the laboratory data used therein. A graphical approach, displaying the relative contribitions of differenct source reactions versus altitude, like that used by Fox and Dalgarno [33], can be of considerable help in identifying assumptions that are especially in need of review.

Acknowledgements: This work was supported by the NASA Mars Data Analysis Program through grant number NNX06AE04G. SRI document MP 08-043.

References:

[1] Barth C. A. et al. (1971) *JGR, 76*, 2213-2227.
[2] Stewart A. I. (1972) *JGR 77*, 54-68.
[3] Barth C. A. et al. (1972a) *Science, 175*, 309-312.
[4] Barth C. A. et al. (1972b) *Icarus, 17*, 457-468.
[5] Stewart A. I. et al. (1972) *Icarus, 17*, 469-474.
[6] Nier A. O. and McElroy M. B. (1977) *JGR, 82*, 4341-4348.
[7] Seiff A. and Kirk D. B. (1977) *JGR, 82*, 4341-4348.
[8] Withers P. et al. (2002) *Icarus, 159*, 259-261.
[9] Izakov M. N. (1978) *Icarus, 36*, 189-197.
[10] Stewart A. J. and Hanson W. B. (1982) *Adv. Space Res. 2*, 87-101.
[11] Culp R. D. and Stewart A. I. (1984) *J. Astronaut. Sci,. 32*, 329-341.
[12] Stewart A.I.F. (1987) "Revised Time Dependent Model of the Martian Atmosphere For Use In Orbit Lifetime and Sustenance Studies," Final Report JPL PO #NQ-802429, 3/26/87.
[13] Justus C. G. and Johnson D. L. (2001) "Mars Global Reference Atmospheric Model 2001 Version (Mars-GRAM 2001): Users Guide," http://trs.nis.nasa.gov/archive/00000549/ .
[14] Keating G. M. et al. (1998) *Science, 279*, 1672-1676.
[15] Tracadas P. W. et al. (2001) *JGR, 106*, E23349.
[16] Magalaes J. A. et al. (1999) *JGR, 104*, E08943.
[17] Tolson R. H. et al. (2005) *J. Spacecraft Rockets 42*, 435-443.
[18] Mazarico E. et al. (2007) *JGR, 112*, E05014.
[19] Bertaux J.-L. et al. (2005a) *Science, 307*, 566-569.
[20] Bertaux J.-L. et al. (2005b) *Nature,435*, 790-794.
[21] Quemerais E. et al. (2006) *JGR, 111*, E09S04.
[22] Leblanc F. et al. (2006) *JGR, 111*, E09S11.
[23] Bertaux J.-L. et al. (2006) *JGR, 111*, E10S90.
[24] Withers P. and Smith M. D. (2006) *Icarus, 185*, 133-142.
[25] Wilson R. J. (2002) *GRL , 29*, 1120.
[26] Forbes J. M. et al. (2002) *JGR, 107*, E05113.
[27] Withers P. et al. (2003) *Icarus, 164*, 14-32.
[28] Angelats i Coll M. et al. (2004) *JGR, 109*, E01011.
[29] Huestis D. L. (2002) *Jacchia 1977 Atmospheric Model* (nssdcftp.gsfc.nasa.gov/models/atmospheric/jacchia/jacchia-77/j77sri.for).
[30] Montmessin F. et al. (2006) JGR, 111, E09809.
[31] LeCompte M. A. et al. (1989) *JGR, 94*, A00208.
[32] Slanger T. G. et al. (2007) "Unpublished Analysis of MEX Data, ESA/NASA Mars Data Analysis Program".
[33] Fox J. L. and Dalgarno A. (1979) *JGR, 84*, A07315.
[34] Simon C. et al. (2008) "Dayglow on Mars: Kinetic Modeling with SPICAM UV Limb Data," (submitted to Planet. Space Sci.).
[35] Shematovich V. I. et al. (2008) *JGR, 113*, E02011.